B16 Vol. 35, No. 10 / October 2018 / Journal of the Optical Society of America B Research Article

Journal of the Optical Society of America B

OPTICAL PHYSICS

Simultaneously spatially and temporally focused femtosecond vortex beams for laser micromachining

WEIBO CHENG,[1] XIAO-LONG LIU,[1,2] AND PAVEL POLYNKIN[1,*]

[1]College of Optical Sciences, The University of Arizona, 1630 East University Boulevard, Tucson, Arizona 85721, USA
[2]Academy of Opto-Electronics, Chinese Academy of Science, Beijing 100094, China
*Corresponding author: ppolynkin@optics.arizona.edu

Received 29 May 2018; revised 9 July 2018; accepted 9 July 2018; posted 30 July 2018 (Doc. ID 332607); published 22 August 2018

We combine conventional beam shaping with simultaneous spatial and temporal focusing (SSTF) to generate femtosecond SSTF vortex beams. We demonstrate the utility of these beam structures by producing single-shot encryption of doughnut-shaped ablation marks on the back surfaces of glass plates. The SSTF enables this type of machining by significantly reducing the nonlinear beam distortions on propagation through the glass.

OCIS codes: (140.3300) Laser beam shaping; (140.3390) Laser materials processing; (320.7110) Ultrafast nonlinear optics.

https://doi.org/10.1364/JOSAB.35.000B16

1. INTRODUCTION

Laser beam shaping has been widely used in diverse areas of science and technology such as optical trapping [1], writing optical waveguides [2], femtosecond laser ablation [3], laser-plasma interaction research [4], and atmospheric science [5,6]. In femtosecond laser ablation, in order to produce material structures with desired properties, various beam shapes have been used, including Bessel beams [7], optical vortices [8], Bessel beams of higher order [9], and Airy beams [10].

Most of the applications in laser micromachining involve ablation of the front surfaces of solid-state materials. When machining inside the bulk or on the back surfaces of transparent dielectrics is sought, spatial and temporal distortions of the laser beam that result from propagation through the nonlinear, dispersive material may worsen the quality of the machined features. For example, it has been shown that machining the back surfaces of glass plates with Bessel beams of higher order, instead of producing smooth ring features that mimic the intensity patterns of the incident beams, produces beaded ring structures. The beading results from the breakup of the originally smooth ring intensity patterns of the laser beams into distinct filaments. This behavior has been attributed to the nonlinearity that accumulates on propagation through the glass [9].

The simultaneous spatial and temporal focusing (SSTF) technique has been developed in order to minimize the cumulative nonlinearity penalty experienced by the beam on propagation through the material. SSTF was first introduced in the context of nonlinear microscopy [11,12] and was later applied to nonlinear optics [13], writing microfluidic channels [14], and ablation of ocular tissue [15].

In the SSTF concept, different spectral components of the incident femtosecond laser pulse are spatially displaced in the transverse beam plane by a dispersive element such as a prism or a grating. If the input beam shape is round, the transformed beam will be elliptical. At any point across the beam, the optical bandwidth is reduced in proportion to the ellipticity of the beam, compared to the bandwidth of the incident beam, where all frequency components of the pulse are spatially overlapping. An objective lens is used to recombine the spatially separated spectrum components. At the focus of the lens, the separated spectral components are spatially overlapping again, and the full bandwidth of the initial pulse is recovered, restoring the initial duration of the femtosecond laser pulse. The shortest pulse duration is achieved only near the focus; thus, the nonlinear beam distortions on propagation towards the focus are significantly reduced.

In this paper, we report the combination of the SSTF technique with conventional beam shaping by generating femtosecond SSTF vortex beams. We experimentally investigate the application of these beams to laser micromachining. We demonstrate the production of highly reproducible, smooth ring structures on the back surfaces of borosilicate glass plates. In contrast, beaded ring structures are produced on the back surfaces of the glass plates, when conventional (without SSTF) vortex beams are used, as a result of nonlinear beam distortions on propagation through the glass.

2. EXPERIMENTAL RESULTS AND DISCUSSION

Our experimental setup is schematically shown in Fig. 1. The laser source is a Ti:sapphire laser system (Libra by Coherent) that delivers 65-fs-long laser pulses with the spectrum centered at around 800 nm in a linearly polarized beam. The repetition rate of the laser is 1 kHz. The pulse energy attainable from the laser system is 4 mJ, which is excessively high for the purposes of the micromachining experiments reported here. Accordingly, the beam is attenuated by a half-wave plate followed by a reflection off a glass wedge at the Brewster's angle. The energy of the attenuated laser pulses is measured with a semiconductor energy sensor.

The laser beam has a nearly perfect Gaussian beam shape with a beam diameter of about 10 mm. We aperture the beam, making the beam shape close to a flat-top with a diameter of 4 mm, immediately after the aperture. The beam is subsequently passed though a third-order fused-silica vortex plate [16]. The plate imposes phase modulation $\propto \exp(im\phi)$ onto the incident flat-phase beam profile. Here, ϕ is the azimuthal angle and $m = 3$ is the order of vorticity. The optical bandwidth of the laser is small enough not to cause any observable distortions of the generated vortex beam due to the wavelength dependence of the phase modulation imposed by the vortex plate [16].

To produce the SSTF beam transformation, we pass the beam through a pair of reflective diffraction gratings with 600 grooves/mm, blazed at 750 nm. The angle of incidence of the beam on both gratings is 32° and the distance between the gratings is 95 mm. After passing through the grating pair, the circular beam shape is transformed into an ellipse with the major and minor axes of 6 mm and 4 mm, respectively. The linear polarization of the beam is parallel to the minor axis of the ellipse. An infinity-corrected microscope objective with a numerical aperture of NA = 0.15 and an entrance pupil diameter of 6 mm is used to recombine the spatially separated spectrum components in the focal plane of the objective. The resulting intensity distribution in the focal plane is doughnut-shaped, with zero intensity on the beam axis. The effects of focusing with high-numerical-aperture focusing optics, discussed in Ref. [17], are insignificant in our focusing geometry.

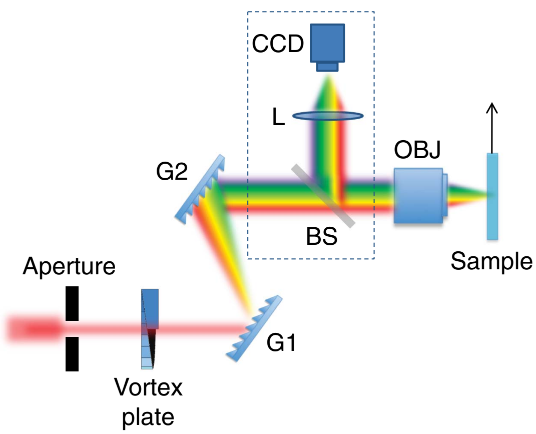

Fig. 1. Schematic of the experimental setup. Vortex plate, order $m = 3$; G1 and G2 are diffraction gratings with a groove density of 600/mm; BS, beam splitter; L, lens with focal length $f = 10$ cm; OBJ, microscope objective with numerical aperture NA = 0.15.

Our micromachining experiments are conducted on borosilicate glass slides with a thickness of 150 μm. The slide is mounted on a computer-controlled, linear motorized translation stage. We investigated both single-shot and multi-shot regimes of ablation. In the case of single-shot micromachining, the stage is translated at a speed of 30 mm/s, resulting in a separation of the ablation sites by about 30 μm. The linear motorized stage is placed on a manual 3D micro-positioning stage, which is used to precisely adjust the position of the focal plane of the microscope objective relative to the sample. The focusing of the SSTF vortex beam on the back surface of the sample is monitored through observing the image of the back reflection from the back surface with a charge-coupled device (CCD) camera. To visualize the results of the micromachining, the sample is sputter-coated with a thin layer of gold and examined under a scanning electron microscope (Hitachi, model S3400N).

The emphasis of the present work is on the micromachining of the back side of the sample, with the laser beam traveling through the glass on the way to the focal plane of the microscope objective. Note that the ablation threshold for the rear surface of the glass side in air is less, by about 30%, than the threshold for ablation of the front surface of the slide. This difference between ablation thresholds for the two surfaces, defined in terms of the incident laser fluence, is due to the constructive interference between the incident and reflected laser beams near the back surface of the sample and destructive interference between the incident and reflected beams near the front surface [18,19].

In order to deliver the shortest pulse to the rear surface, the input pulse is positively chirped, thus compensating for the negative chirp introduced by the gratings in the SSTF setup, the beam splitter, the objective lens, and the glass slide. Dispersion compensation is optimized by maximizing the visible fluorescence that results from the ionization of glass at the focal plane of the lens, with the focal point advanced slightly into the glass [14].

As mentioned above, we investigated both single-shot and multi-shot regimes of ablation. The results of single-shot micromachining with SSTF vortex beams are shown in Fig. 2. With the focusing and pulse compression optimized at the back side of the glass slide, the onset of visible material modification occurs at an energy of the incident laser pulse of about 6 μJ. At higher values of pulse energy, the interaction of the laser pulse with the back surface of the slide results in the formation of a smooth, doughnut-shaped ablation feature. That is a clear

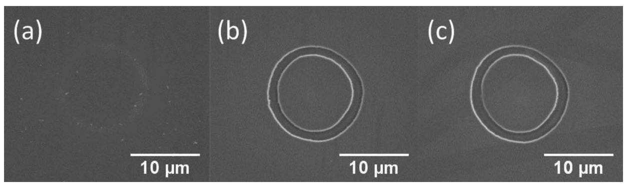

Fig. 2. Single-shot ablation marks produced on the back surfaces of borosilicate glass plates with SSTF vortex beams. The order of vorticity $m = 3$. For the three cases shown, the pulse energy is (a) 6 μJ, (b) 13 μJ, and (c) 17 μJ.

indication of the nearly perfect recombination of the spatially separated spectral beamlets of the SSTF beam at the focal plane of the objective. Note that the appearance of the doughnut ablation feature is relatively insensitive to the energy of the laser pulse, as long as it is above the threshold value of 6 μJ, in our focusing geometry. For pulse-energy values significantly exceeding the threshold value, modifications within the bulk and on the front surface of the sample start to appear.

To investigate multi-shot micromachining with SSTF vortex beams, we subjected the back side of the glass slide to the cumulative effect of about 1000 laser pulses. An image of the machined feature, obtained with 1 μJ energy of the laser pulses within the 1000-pulse sequence, is shown in Fig. 3. The formation of nano-gratings with a period of about 700 nm within the doughnut-shaped ablation feature is evident in the image. The direction of the grooves in the nano-grating is perpendicular to the direction of polarization of the laser. Discussion of the nano-grating formation [20–22] is outside of the scope of this paper.

To highlight the enabling role of the SSTF focusing, we attempted to produce ablation features on the back surfaces of glass slides, using conventional vortex beams (without SSTF), under otherwise the same conditions as those used in the experiments with SSTF vortices discussed above. To that end, we replaced the grating pair used in the SSTF setup with a pair of mirrors and adjusted the pulse compressor in the laser to deliver a temporally compressed and focused vortex beam to the back side of the glass slide. Under these conditions, the regular vortex beam of order $m = 3$ was found to be unable to produce any visible ablation marks on the back surface of the glass slide in the single-shot regime with any energy of the incident laser pulse. We argue that this inability of the regular vortices to ablate the back surface of the glass sample under the conditions of our experiment is due to the premature beam self-focusing inside the glass on the way towards the focal plane, and, for very high values of pulse energy, due to the ablation of the front surface of the sample.

The above conclusion is supported by experiments on ablation of the back surfaces of the glass slides with regular vortex beams (without SSTF) in the multi-shot regime. The results of these experiments are shown in Fig. 4. Here, the ablation sites were illuminated for one second, corresponding to about 1000 laser shots consecutively hitting the same position on the sample. The resulting doughnut-shaped ablation features are fragmented into discrete spots. When the energy of individual laser pulses within the pulse sequence is increased, the number of the individual spots that the doughnut-shaped feature is fragmented into decreases, as shown in Fig. 4(b). The spots finally disappear altogether at yet higher values of the laser-pulse energy, as the beam fragmentation occurs deeper inside the glass slide, before the beam reaches the back side of the sample, as shown in Fig. 4(c).

The conclusion on the fragmentation of the smooth doughnut-shaped intensity features of the ordinary vortex beams due to self-focusing inside the glass slide is further supported by the following estimate. The critical power for the *self-similar* collapse of a continuous-wave vortex beam of order m, in glass, can be estimated as $P_{\mathrm{cr}}^{(m)} \approx 2\sqrt{3}mP_{\mathrm{cr}}^{(0)}$ [23], where $P_{\mathrm{cr}}^{(0)}$ is the critical power for the self-focusing collapse of a Gaussian beam. It has been analytically and experimentally shown that the fragmentation of the vortex ring-intensity feature into discrete filaments, due to the azimuthal modulation instability, occurs at a peak power significantly lower than that for the self-similar collapse of the ring [6,24]. Thus, the self-similar collapse can only happen in the case of an ideal vortex beam, without any amplitude or phase perturbations. In glass at an 800 nm wavelength, $P_{\mathrm{cr}}^{(0)} \approx 2.5$ MW [25]; thus, $P_{\mathrm{cr}}^{(3)} \approx 26$ MW. As we found previously (Fig. 2), the pulse-energy threshold for the formation of an ablation mark on the back side of the glass slide with an SSTF vortex beam of order 3, under our experimental conditions, is 6 μJ. Given the 65 fs duration of the laser pulse, this threshold pulse energy corresponds to peak power in excess of 90 MW. Thus, an ordinary vortex beam (without SSTF), in our setup, with the energy that would be sufficient to produce ablation, carries significantly higher peak power than the threshold for the azimuthal breakup of the vortex ring into individual filaments. The beam breakup, occurring inside the glass on the way to the focus on the back side of the sample, distorts the beam and prevents it from producing an ablation feature in the single-shot regime at any level of pulse energy. The nonlinear azimuthal breakup of vortex beams has been previously observed in glass [9], water [26,27], and air [6].

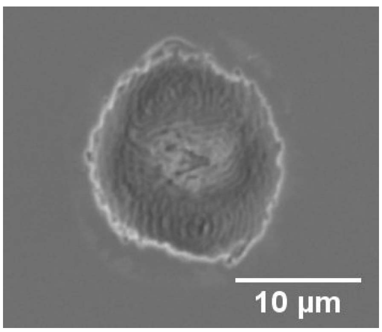

Fig. 3. Ablation feature produced on the back surface of a borosilicate glass plate through multi-shot micromachining with an SSTF vortex beam. The ablation site is exposed to 1000 laser shots with the energy of an individual laser pulse of about 1 μJ. Other conditions are the same as those in the single-shot micromachining experiments shown in Fig. 2.

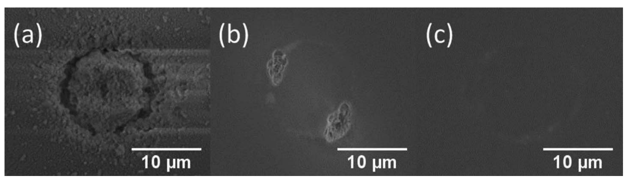

Fig. 4. Results of multi-shot micromachining of the back sides of the borosilicate glass slides with the ordinary (without SSTF) vortex beams focused and temporally compressed on the back side of the sample. The order of vorticity is $m = 3$. In all cases shown, the ablation sites are exposed to about 1000 laser shots separated by 1 ms. Different cases correspond to different values of energy of the laser pulses within the 1000-pulse sequence: (a) 9 μJ, (b) 21 μJ, and (c) 25 μJ. In (a), the azimuthal breakup of the ring intensity feature occurs immediately before the beam reaches the back surface of the glass slide. As the pulse energy is increased, the azimuthal breakup of the vortex ring occurs deeper inside the glass, and the beaded ablation feature on the back surface of the sample eventually disappears.

3. CONCLUSION

In conclusion, we have experimentally synthesized femtosecond SSTF vortex beams, by combining conventional beam shaping using a phase plate with SSTF beam focusing. We have demonstrated that these beams have practical utility by producing single-shot doughnut ablation features on the back sides of glass plates. Contrary to the case of the SSTF vortex beam, a regular vortex (without the SSTF), under otherwise the same conditions, was unable to propagate through the glass to the back side of the sample while maintaining its smooth doughnut-shaped intensity feature. In that case, the azimuthal beam breakup prevented the beam from producing any ablation marks in the single-shot regime, even at a much higher level of pulse energy than what was used to successfully ablate the sample with the SSTF vortex.

Funding. Air Force Office of Scientific Research (AFOSR) (FA9550- 12-1-0482, FA9550-16-1-0013).

Acknowledgment. The authors thank Prof. Thomas D. Milster, Mr. Victor Densmore III, and Mr. Caleb Baker for technical assistance.

REFERENCES

1. K. T. Gahagan and G. A. Swartzlander, “Optical vortex trapping of particles,” Opt. Lett. **21**, 827–829 (1996).
2. R. Osellame, S. Taccheo, M. Marangoni, R. Ramponi, P. Laporta, D. Polli, S. De Silvestri, and G. Cerullo, “Femtosecond writing of active optical waveguides with astigmatically shaped beams,” J. Opt. Soc. Am. B **20**, 1559–1567 (2003).
3. P. Polynkin, “Intense femtosecond shaped laser beams for writing extended structures inside transparent dielectrics,” Appl. Phys. A **114**, 143–149 (2014).
4. J. Fan, E. Parra, I. Alexeev, K. Y. Kim, H. M. Milchberg, L. Y. Margolin, and L. N. Pyatnitskii, “Tubular plasma generation with a high-power hollow Bessel beam,” Phys. Rev. E **62**, R7603 (2000).
5. P. Polynkin, M. Kolesik, A. Roberts, D. Faccio, P. DiTrapani, and J. Moloney, “Generation of extended plasma channels in air using femtosecond Bessel beams,” Opt. Express **16**, 15733–15740 (2008).
6. P. Polynkin, C. Ament, and J. V. Moloney, “Self-focusing of ultraintense femtosecond optical vortices in air,” Phys. Rev. Lett. **111**, 023901 (2013).
7. M. K. Bhuyan, M. K. F. Courvoisier, P. A. Lacourt, M. Jacquot, R. Salut, L. Furfaro, and J. M. Dudley, “High aspect ratio nanochannel machining using single shot femtosecond Bessel beams,” Appl. Phys. Lett. **97**, 081102 (2010).
8. C. Hnatovsky, V. G. Shvedov, W. Krolikowski, and A. V. Rode, “Materials processing with a tightly focused femtosecond laser vortex pulse,” Opt. Lett. **35**, 3417–3419 (2010).
9. W. Cheng and P. Polynkin, “Micromachining of borosilicate glass surfaces using femtosecond high-order Bessel beams,” J. Opt. Soc. Am. B **31**, C48–C52 (2014).
10. A. Mathis, F. Courvoisier, L. Froehly, L. Furfaro, M. Acquot, P. A. Lacourt, and J. M. Dudley, “Micromachining along a curve: femtosecond laser micromachining of curved profiles in diamond and silicon using accelerating beams,” Appl. Phys. Lett. **101**, 071110 (2012).
11. D. Oron, E. Tal, and Y. Silberberg, “Scanningless depth-resolved microscopy,” Opt. Express **13**, 1468–1476 (2005).
12. G. Zhu, J. van Howe, M. Durst, W. Zipfel, and C. Xu, “Simultaneous spatial and temporal focusing of femtosecond pulses,” Opt. Express **13**, 2153–2159 (2005).
13. G. Li, J. Ni, H. Xie, B. Zeng, J. Yao, W. Chu, H. Zhang, C. Jing, F. He, H. Xu, Y. Cheng, and A. Xu, “Second harmonic generation in centrosymmetric gas with spatiotemporally focused intense femtosecond laser pulses,” Opt. Lett. **39**, 961–964 (2014).
14. F. He, H. Xu, Y. Cheng, J. Ni, H. Xiong, Z. Xu, K. Sugioka, and K. Midorikawa, “Fabrication of microfluidic channels with a circular cross section using spatiotemporally focused femtosecond laser pulses,” Opt. Lett. **35**, 1106–1108 (2010).
15. E. Block, M. Greco, D. Vitek, O. Masihzadeh, D. A. Ammar, M. Y. Kahook, N. Mandava, C. Durfee, and J. Squier, “Simultaneous spatial and temporal focusing for tissue ablation,” Biomed. Opt. Express **4**, 831–841 (2013).
16. C. Ament, L. Johnson, A. Schmitt-Sody, A. Lucero, T. Milster, and P. Polynkin, “Generation of multiterawatt vortex laser beams,” Appl. Opt. **53**, 3355–3360 (2014).
17. B. Chen, J. Pu, and O. Korotkova, “Focusing of a femtosecond vortex light pulse through a high numerical aperture objective,” Opt. Express **18**, 10822–10827 (2010).
18. R. Boyd, *Nonlinear Optics*, 3rd ed. (Academic, 2008).
19. W. Lowdermilk and D. Milam, “Laser-induced surface and coating damage,” IEEE J. Quantum Electron. **17**, 1888–1903 (1981).
20. Y. Shimotsuma, P. Kazansky, J. Qiu, and K. Hirao, “Self-organized nanogratings in glass irradiated by ultrashort light pulses,” Phys. Rev. Lett. **91**, 247405 (2003).
21. R. Buividas, M. Mikutis, and S. Juodkazis, “Surface and bulk structuring of materials by ripples with long and short laser pulses: Recent advances,” Prog. Quantum Electron. **38**, 119–156 (2014).
22. C. Hnatovsky, V. Shvedov, W. Krolikowski, and A. Rode, “Revealing local field structure of focused ultrashort pulses,” Phys. Rev. Lett. **106**, 123901 (2011).
23. G. Fibich and N. Gavish, “Critical power of collapsing vortices,” Phys. Rev. A **77**, 045803 (2008).
24. A. Vincotte and L. Berge, “Femtosecond optical vortices in air,” Phys. Rev. Lett. **95**, 193901 (2005).
25. T. Pitts, T. Luk, J. Gruetzner, T. Nelson, A. McPherson, S. Cameron, and A. Bernstein, “Propagation of self-focusing laser pulses in atmosphere: experiment versus numerical simulation,” J. Opt. Soc. Am. B **21**, 2008–2016 (2004).
26. L. T. Vuong, T. D. Grow, A. Ishaaya, A. L. Gaeta, G. W. ’t Hooft, E. R. Eliel, and G. Fibich, “Collapse of optical vortices,” Phys. Rev. Lett. **96**, 133901 (2006).
27. S. Shiffler, P. Polynkin, and J. Moloney, “Self-focusing of femtosecond diffraction-resistant vortex beams in water,” Opt. Lett. **36**, 3834–3836 (2011).